Carbon 113 (2017) 151–158

Contents lists available at ScienceDirect

Carbon

journal homepage: www.elsevier.com/locate/carbon

Flexible all-solid-state asymmetric supercapacitor based on transition metal oxide nanorods/reduced graphene oxide hybrid fibers with high energy density

Wujun Ma, Shaohua Chen, Shengyuan Yang, Wenping Chen, Wei Weng, Yanhua Cheng, Meifang Zhu*

State Key Laboratory for Modification of Chemical Fibers and Polymer Materials, College of Materials Science & Engineering, Donghua University, 2999 North Renmin Road, Shanghai 201620, China

ARTICLE INFO

Article history:
Received 16 October 2016
Received in revised form
15 November 2016
Accepted 19 November 2016
Available online 19 November 2016

ABSTRACT

Fiber-shaped flexible supercapacitors have attracted considerable attention in recent years due to their potential application in wearable electronics. However, the limited energy density is still a serious bottleneck which restricts their practical application. In this work, transition metal oxide nanorods/reduced graphene oxide (rGO) hybrid fibers were prepared by a facile, scalable wet-spinning method. Due to the synergetic effects between transition metal oxide nanorods and rGO, the electrochemical performance of the hybrid fibers were greatly improved. An all-solid-state asymmetric supercapacitor was constructed by using MnO_2 nanorods/rGO hybrid fiber as positive electrode, MoO_3 nanorods/rGO hybrid fiber as negative electrode and H_3PO_4/poly(vinyl alcohol) (PVA) as electrolyte. Based on the different working potential window between MnO_2 and MoO_3, the optimized asymmetric supercapacitor can be cycled reversibly at a high voltage of 1.6 V and deliver a superior volumetric energy density of 18.2 mWh cm^{-3} at a power density of 76.4 mW cm^{-3}. Besides, the asymmetric supercapacitor exhibits remarkable cycling stability and excellent flexibility and mechanical stability.

1. Introduction

The rapid advances in portable and wearable electronics have triggered intensive research efforts on lightweight, flexible and highly efficient energy storage systems [1–6]. Thanks to their superior power density and long cycle life, supercapacitors (SCs) are highly desirable as an important class of energy storage systems [7–9]. In the past few years, considerable efforts have been dedicated to developing fiber-shaped SCs (FSCs) owing to their superior features such as lightweight, tiny volume, flexibility, and knittability [10–17]. Among different FSCs, graphene fiber as a new type of carbon fiber is broadly regarded to be promising electrode due to its high strength, low weight and outstanding flexibility [18,19]. Despite the recent progress in graphene fiber-based SCs, the limited energy density is still a serious bottleneck which restricts their practical application [20–25]. Therefore, it is highly desirable to improve their energy density to meet the demands of wearable electronics [26].

According to the equation $E = 1/2CV^2$, the energy density (E) can be improved by either increasing the device capacitance (C) and/or the operation voltage (V) [27]. To date, research on FSCs has been focused mostly on increasing the C with a narrow V of less than 1 V and insufficient attention has been paid to increase the voltage range [28,29]. A promising strategy to increase operation voltage is to construct asymmetric supercapacitors (ASCs) by using two appropriate electrodes with different potential windows [30].

The electrochemical properties of SCs are usually affected by the properties and structures of their electrode materials. Therefore, developing high-energy density ASCs mainly depends on the selection and fabrication of appropriate electrode materials [31]. Compared with carbon-based materials, pseudo-capacitive materials such as transition metal oxides and conducting polymers exhibit much higher capacitive performance [32]. Incorporation of pseudo-capacitive materials with graphene fibers has been demonstrated to be an effective way to enhance the specific capacitance, and, in turn, the device energy density [33–35]. However, in previously reported ASCs, carbonaceous materials with

* Corresponding author.
E-mail address: zhumf@dhu.edu.cn (M. Zhu).

http://dx.doi.org/10.1016/j.carbon.2016.11.051
0008-6223/

lower specific capacitances were usually applied as negative electrode and transition metal oxides were used as positive electrode. Few studies focused on constructing an ASC based on transition metal oxides in both electrodes [26,36].

In the work described herein, we successfully prepared MoO_3 nanorods/rGO and MnO_2 nanorods/rGO hybrid fibers through a facile, scalable wet-spinning method. The one-dimensional nanorods can give full play to the electrochemical performance of the transition metal oxides due to their shortened diffusion length and large interface area. Meanwhile, the nanorods in the fiber can act as an effective spacer to prevent the restacking of graphene nanosheets and provide more accessible surface area. Additionally, graphene with high electrical conductivity can improve the electrical conductivity of the hybrid fibers and facilitate charge transport in the electrode, improving the pseudocapacitive reactions and rate capability. An all-solid-state ASC was constructed by using MnO_2 nanorods/rGO hybrid fiber as the positive electrode and MoO_3 nanorods/rGO hybrid fiber as the negative electrode. Based on the different working potential window between MnO_2 and MoO_3, the optimized ASC can be cycled reversibly at a high voltage of 1.6 V and deliver a superior volumetric energy density of 18.2 mWh cm^{-3} at a power density of 76.4 mW cm^{-3}. Besides, the ASC exhibits remarkable cycling stability and excellent flexibility and mechanical stability.

2. Experimental section

2.1. Preparation of flexible negative electrodes (MoO_3 nanorods/rGO hybrid fiber)

Graphite oxide (GO) was synthesized by using the modified Hummers method [37]. MoO_3 nanorod was prepared through a hydrothermal method (see Supplementary Material). To obtain MoO_3 nanorods/rGO hybrid fibers, 180 mg GO was firstly dispersed into 20 ml distilled water, sonicated for 1 h (45 W), then 20 mg MoO_3 nanorods were added into the solution, and sonicated for another 1 h, finally the solution was concentrated to 20 mg ml^{-1} in a water bath at 60 °C. The dispersion was injected into a rotating coagulation bath composed of acetic acid. The obtained MoO_3 nanorods/GO hybrid gel fibers were dried at 80 °C. To obtain MoO_3 nanorods/rGO hybrid fiber, the hybrid fiber was annealed under Ar atmosphere at 600 °C for 3 h. By the same method, a series of hybrid fibers were prepared with MoO_3 content of 10%, 20%, 40% and 60%, respectively named as MoO_3/rGO-10, MoO_3/rGO-20, MoO_3/rGO-40 and MoO_3/rGO-60.

2.2. Preparation of flexible positive electrodes (MnO_2 nanorods/rGO hybrid fiber)

MnO_2 nanorods were prepared by using a hydrothermal method. MnO_2 nanorods/GO hybrid fiber was fabricated according to the above method. MnO_2 nanorods/rGO hybrid fiber was obtain according to our previous work [33].

2.3. Characterization

The morphology of the fiber was investigated using scanning electron microscope (SEM) (HITACHI, S4800). The compositions of the hybrid fibers were studied by using Raman spectra (Renishaw microRaman, 514.5 nm laser), X-ray diffraction (XRD) patterns (D/max 2550 Rigaku, Japan) and X-ray photoelectron spectroscopy (XPS) (Axis Ultra DLD spectrometer, Kratos Analytical, UK). The mechanical properties of the fiber were carried out on an XQ-1A fiber tension tester (Shanghai New Fiber Instrument).

2.4. Electrochemical characterization of individual fiber electrodes

The fiber electrode was prepared by connecting a fiber to stainless steel strip end to end by silver paste. Electrochemical tests were performed using a three-electrode system on CHI 660E electrochemical workstation in 1 M H_2SO_4 electrolyte. Fiber electrode, a Pt wire and Hg/Hg_2SO_4 electrode were used as the working, counter and reference electrode, respectively. The volumetric capacitance was calculated through the CV curves by the following equation

$$C_V = \frac{1}{2V\Delta U\nu}\int I dU \tag{1}$$

where C_V is the specific capacitance, ΔU is the potential window, ν is the scan rate, I is the current, V is the volume of the fiber electrode which can be calculated using the equation

$$V = \pi R^2 L \tag{2}$$

where R and L are the radius and length of the fiber, respectively.

2.5. Fabrication of all-solid-state supercapacitor and electrochemical measurements

To fabricate a fiber-based ASC, a MoO_3 nanorods/rGO hybrid fiber and a MnO_2 nanorods/rGO hybrid fiber were coated with H_3PO_4/PVA gel electrolyte, respectively, solidified at room temperature, and then the two electrodes were carefully twisted together. Finally a layer of H_3PO_4/PVA was coated on the SC. The electrochemical studies of the ASC were carried out in a two-electrode system. The volumetric capacitance of the ASC was calculated from CV curves using the equation

$$C_V = \frac{1}{2V\Delta U\nu}\int I dU \tag{3}$$

where C_V is the total volumetric capacitance, V is the total volume of the SC including positive and negative electrodes.

The volumetric energy (E_V) and power (P_V) density of the ASC can be obtained from the following equation

$$E_V = \frac{1}{2}C_V \Delta U^2 \tag{4}$$

$$P_V = E_V/\Delta t \tag{5}$$

3. Results and discussion

For ASCs constructed from two different transition metal oxide electrodes, the working potential window is directly related to their work function difference [26]. Therefore, we choose MnO_2 and MoO_3 as the positive and negative electrodes, respectively, due to their largest work function difference [38]. To fabricate fiber based electrodes, a facile wet spinning method based on our previous work was used [33]. Fig. 1 shows the schematic illustration of the fabrication processes of different fiber based electrodes and the design of the solid-state ASC.

3.1. Negative electrode materials

The morphology and microstructure of the MoO_3/rGO fiber was characterized using SEM. Fig. 2a shows that the obtained hybrid fiber has a circular cross-section, and the diameter is about 25 μm.

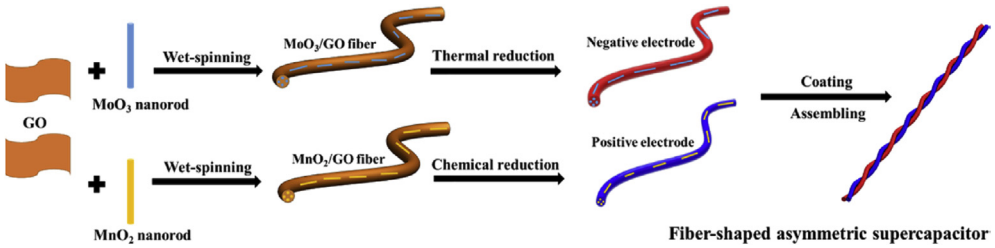

Fig. 1. Schematic illustration of the design and fabrication of the fiber-based ASC. (A colour version of this figure can be viewed online.)

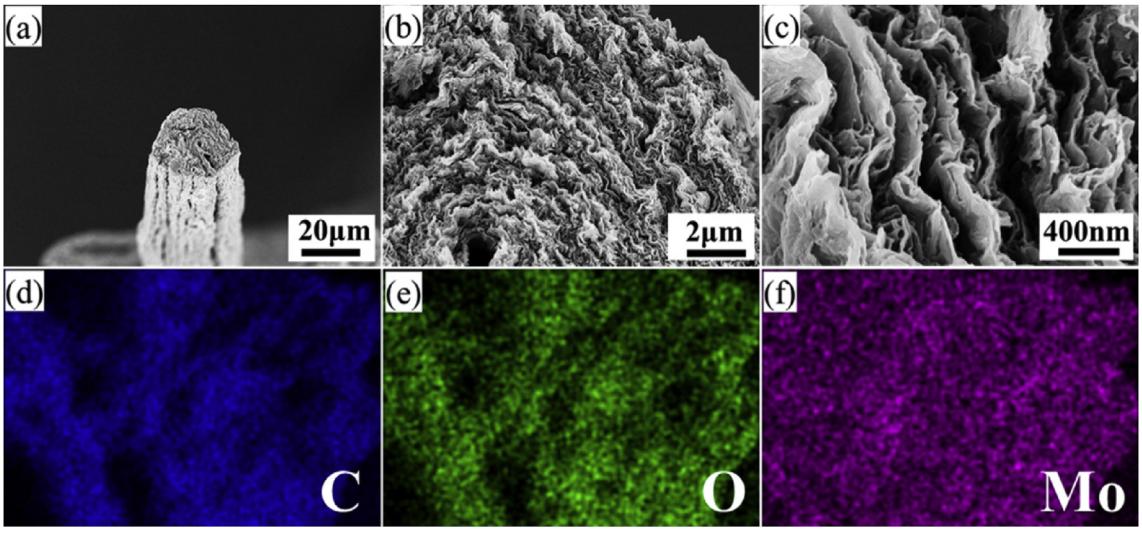

Fig. 2. (a–c) SEM images of the cross-section of the MoO_3/rGO hybrid fiber. (d-f) EDS mappings of C, O and Mo elements for the hybrid fiber. (A colour version of this figure can be viewed online.)

Within the hybrid fiber, the rGO layers interconnect each other and align along the axial direction (Fig. 2b), which provide a conductive network for electronic transport. Meanwhile, the rGO sheets were well-separated and formed porous structure with a low density (1.14 g cm^{-3}) (Fig. 2c), thus the hybrid fiber has a specific surface area of 130.5 m^2 g^{-1} and the pore size distribution ranges from 2.5 nm to 50 nm (Fig. S2). The hybrid fiber with porous structure can provide more accessible surface area and easy pathways for fast electrolyte ions diffusion, thus achieving high capacitance and low charge transfer resistance [39]. The elemental distribution of the hybrid fiber was acquired through EDS mapping of the cross-section (Fig. 2d–f), in which C, O, Mo elements are uniformly distributed, suggesting a homogeneous distribution of MoO_3 nanorods in the hybrid fiber.

Interconnected rGO sheets in the hybrid fiber can act as mechanical support and electron transport channel for the fiber, resulting in good electrical and mechanical properties. The tensile strength of the neat rGO fiber is about 180 MPa and decreases to 98 MPa with the MoO_3 content increasing to 60%, which could be attributed to the formed pores in the hybrid fiber (Fig. S3a). The strength of the hybrid fibers is higher than that of rGO fiber (49.3 MPa) [20], SWCNT/rGO fiber (84 MPa) [11], graphene porous fibers (11.1 MPa) [40] and GO@CMC fiber (73 MPa) [23]. Due to the low conductivity of MoO_3, the conductivity of the hybrid fibers also decreases (from 29.2 S cm^{-1} to 16.8 cm^{-1}) with the increasing amount of MoO_3 nanorods (Fig. S3b).

The obtained MoO_3/rGO hybrid fiber and MoO_3 were characterized by Raman spectroscopy (Fig. 3a). For MoO_3 nanorods, the typical Raman bands at 995 cm^{-1}, 817 cm^{-1} and 664 cm^{-1} could be assigned to the stretching vibrations of the Mo=O and O–Mo–O bonds, consistent with previous reports [41,42]. For MoO_3/rGO hybrid fiber, the characteristic Raman peaks of MoO_3 and rGO were observed simultaneously, indicating the successful fabrication of MoO_3/rGO hybrid fiber [43]. Furthermore, the MoO_3/rGO hybrid fiber and pure MoO_3 were further characterized by XRD spectrum (Fig. 3b). The typical XRD pattern of pure MoO_3 confirmed the formation of orthorhombic structure (α-MoO_3, JCPDS No.05-0508), and the sharp diffraction peaks indicate its high crystallinity [26]. For the MoO_3/rGO hybrid fiber, the typical XRD peak of rGO was not observed clearly, which could be attributed to the low stacking degree of rGO nanosheets in the hybrid fiber as shown in the SEM images (Fig. 2).

The obtained fibers with high mechanical strength and electrical conductivity were directly used as freestanding working electrode without any type of current collectors. In order to study the impact of MoO_3 content on the electrochemical performance, a series of hybrid fiber with different amount of MoO_3 were fabricated. The electrochemical characteristics of the fiber electrode were investigated by using a three electrode system in 1.0 M H_2SO_4 electrolyte. Fig. 4a shows the representative CV curves measured at 10 mV s^{-1}. A pair of well-defined redox peaks related to reversible oxidation state change of Mo element between Mo (IV) and Mo (VI) can be obviously observed in the curves of the hybrid fiber electrodes, indicating the existence of pseudocapacitance [43]. The CV curves display enlarging areas with the increase of MoO_3 content, which is due to the double layer contribution of well-separated graphene along with the pseudocapacitive contribution of MoO_3. Fig. 4b gives the galvanostatic charge/discharge (GCD) curves at a constant

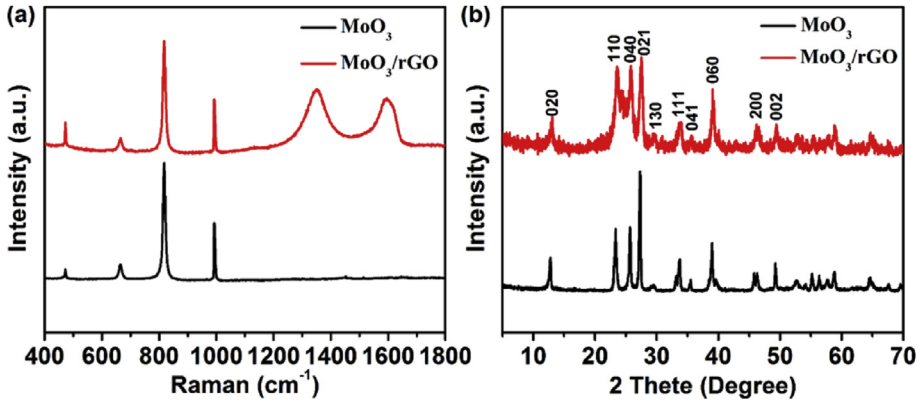

Fig. 3. Raman (a) and XRD (b) spectra of the MoO_3/rGO fiber and the MoO_3 nanorods. (A colour version of this figure can be viewed online.)

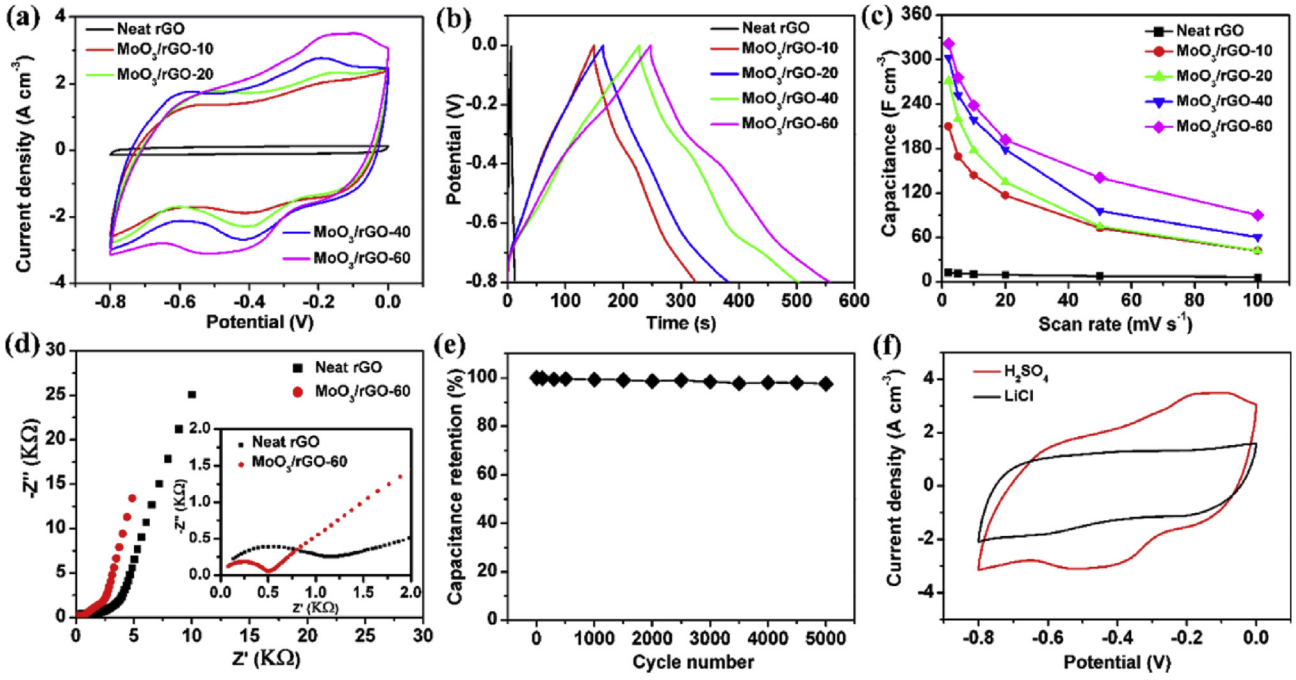

Fig. 4. Electrochemical performance of the neat rGO and MoO_3/rGO hybrid fiber electrode. (a) CV curves at 10 mV s^{-1}. (b) Galvanostatic charge/discharge curves at 1 A cm^{-3}. (c) Specific capacitance as function of scan rate. (d) Nyquist plots. (e) Cycle performance of MoO_3/rGO hybrid fiber electrode at 1 A cm^{-3}. (f) Comparative CV curves of MoO_3/rGO-60 fiber in 1 M LiCl and H_2SO_4 at a scan rate of 10 mV s^{-1}. (A colour version of this figure can be viewed online.)

current density of 1 A cm^{-3}, from which two obvious voltage plateaus are well observed for the MoO_3/rGO hybrid fiber electrodes, which is consistent with the CV curves. It also reveals that the charge curves are almost symmetrical with their corresponding discharge curves with a less obvious voltage drop, indicating small internal resistance and excellent capacitive behavior of the MoO_3/rGO fiber electrodes. The volumetric capacitance for different MoO_3 contents was plotted versus the scan rate in Fig. 4c. The capacitance of neat rGO fiber electrode is 12.5 F cm^{-3}, and increases with MoO_3 mass loading. The highest capacitance (321.8 F cm^{-3}) was obtained from MoO_3/rGO-60 fiber electrode at a scan rate of 2 mV s^{-1}. When the scan rate increases to 100 mV s^{-1}, the volumetric capacitance of MoO_3/rGO-60 fiber electrode reduces to 90.1 F cm^{-3} due to the relatively insufficient Faradaic redox reaction at high scan rate [44]. The volumetric capacitance of MoO_3/rGO-60 fiber electrode is much higher as compared to other fiber-based SCs reported up to date [20,21,28,34,45]. Fig. 4d presents the Nyquist plots of neat rGO and MoO_3/rGO-60 fiber electrode. It is apparent that the equivalent series resistance of MoO_3/rGO-60 is smaller than neat rGO fiber, though the conductivity of neat rGO fiber is higher than MoO_3/rGO-60 hybrid fiber. The reduced equivalent series resistance of MoO_3/rGO-60 could be ascribed to the introduction of MoO_3 nanorods which prevented the restacking of graphene nanosheets and formed porous structure in the hybrid fiber and the porous structure is capable of facilitating the fast diffusion of electrolyte ions into the hybrid fiber electrode [46]. The cycle life of MoO_3/rGO-60 electrode was tested through GCD with a fixed current density of 1 A cm^{-3} (Fig. 4e). It retained 97.6% of its initial specific capacitance after 5000 cycles, indicating good long-term cycle stability. The CV curve shows redox peaks versus Hg/Hg_2SO_4 in 1.0 M H_2SO_4, indicating the presence of pseudocapacitance. The redox peaks disappear in neutral electrolyte (1 M LiCl) (Fig. 4f), suggesting that the pseudocapacitance was induced by MoO_3 nanorods. The clearly improved electrochemical performance of the MoO_3/rGO hybrid

fiber electrode can be attributed to the pseudocapacitance derived from MoO_3 nanorods and the formed porous structure which could provide more accessible surface area for the electrolyte ions and allow fast diffusion of electrolyte ions in the hybrid fibers.

3.2. Positive electrode materials

MnO_2 nanorods/rGO hybrid fiber was prepared by a facile wet spinning method, the mass content of the MnO_2 nanorods is about 40% and the density of the hybrid fiber is about 1.06 g cm^{-3}. The Raman spectra and XPS (Fig. S6) revealed that the MnO_2/rGO hybrid fiber was successfully prepared. The electrochemical performance was investigated by using a three electrode cell in 1.0 M H_2SO_4. Fig. 5a shows the CV curves of the neat rGO and MnO_2/rGO hybrid fiber at a scan rate of 10 mV s^{-1}. The larger area of MnO_2/rGO hybrid fiber as compared to the neat rGO fiber indicates that the introduction of MnO_2 nanorods can improve the capacitive behavior of rGO fiber. The MnO_2/rGO hybrid fiber shows symmetrical rectangular shape CV curves at various scan rates (Fig. 5b), indicating its good capacitive behavior due to the electrical double layer charge storage of rGO along with the fast, reversible and successive redox reactions of MnO_2 nanorods. Fig. 5c displays the capacitance of the MnO_2/rGO hybrid fiber electrode versus scan rates. The highest capacitance is 281.3 F cm^{-3} at 2 mV s^{-1}. As the scan rate increases to 100 mV s^{-1}, the capacitance reduces to 135.1 F cm^{-3} with capacitance retention of about 48%, demonstrating its good rate capability. The capacitance of MnO_2/rGO hybrid fiber is superior to other MnO_2/carbon fiber-based electrodes in the literature [28,47]. The remarkable enhancement of the performance for MnO_2/rGO fiber electrode can be attributed to the synergetic effects between the pseudocapacitance of MnO_2 nanorods and the electric double-layer capacitance of rGO in the hybrid fiber. Fig. 5d displays the long cycling stability of the MnO_2/rGO fiber electrode. After 5000 cycles, it remained 96.6% of its initial value, proving its outstanding cycling performance.

3.3. All-solid-state asymmetric supercapacitor

An all-solid-state ASC was constructed using MnO_2 nanorods/rGO hybrid fiber as the positive electrode and MoO_3 nanorods/rGO hybrid fiber as the negative electrode, which was shown in Fig. 6 b. To achieve the maximum performance of the ASC device, the charge between the positive and the negative electrodes should be balanced, which follows the relationship $q_+ = q_-$ [48]. However, the commonly used gravimetric capacitance is not applicable to the fiber electrode due to its small mass and unique one dimensional configuration. Thus, we use length capacitance to balance the charge between the two fiber electrodes. Fig. S7 shows the length capacitance of MnO_2 nanorods/rGO fiber and MoO_3 nanorods/rGO fiber. It reveals that the capacitance difference between the two electrodes is negligible. Therefore, we selected two hybrid fibers with the same length to construct the ASC. Fig. 6 a shows that the stable voltage windows of the MoO_3/rGO and MnO_2/rGO electrodes were −0.8 to 0 V and 0–0.8 V (vs Hg/Hg_2SO_4), respectively. Thus, it is expected that the operation voltage could be extended to 1.6 V for the proposed asymmetric ASC. Fig. 6c and Fig. S8 show the CV and GCD curves in different voltage windows, respectively. Indeed, the fabricated ASC exhibits a stable operating window up to 1.6 V. Fig. 6d shows the volumetric capacitance of the ASC with the increase of potential window. The specific capacitance significantly increases from 26.9 to 42.8 F cm^{-3} as the potential increases from 0.8 to 1.6 V. Fig. 6e shows the CV curves of the ASC at various scan rates from 5 to 100 mV s^{-1} and the typical faradaic pseudocapacitive shape was observed at low scan rate, manifesting the fast redox reactions of the metal oxide nanorods. Fig. 6f shows the corresponding specific capacitance at various scan rates. The specific capacitance of the device was 51.2 F cm^{-3} at 2 mV s^{-1} and it reduced to 19.4 F cm^{-3} with the scan rate increases to 100 mV s^{-1}. Furthermore, the volumetric capacitance of the ASC at various current density was also calculated based on the GCD curves (Fig. S9). A high volumetric capacitance of 53.5 F cm^{-3} was achieved at a current density of 100 mA cm^{-3}, when the current density

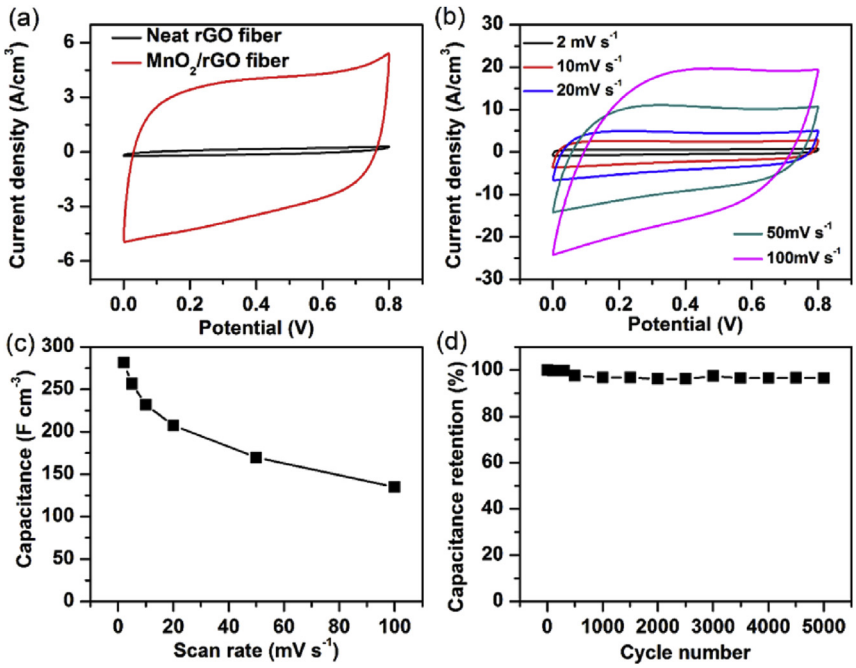

Fig. 5. Electrochemical performance of the neat rGO and MnO_2 nanorods/rGO hybrid fiber electrode. (a) CV curves of rGO and MnO_2/rGO fiber at 10 mV s^{-1} (b) CV curves of MnO_2/rGO fiber at various scan rates. (c) Volumetric capacitance of MnO_2/rGO fiber at different scan rates. (d) Cycling performance of MnO_2/rGO fiber at 1 A cm^{-3}. (A colour version of this figure can be viewed online.)

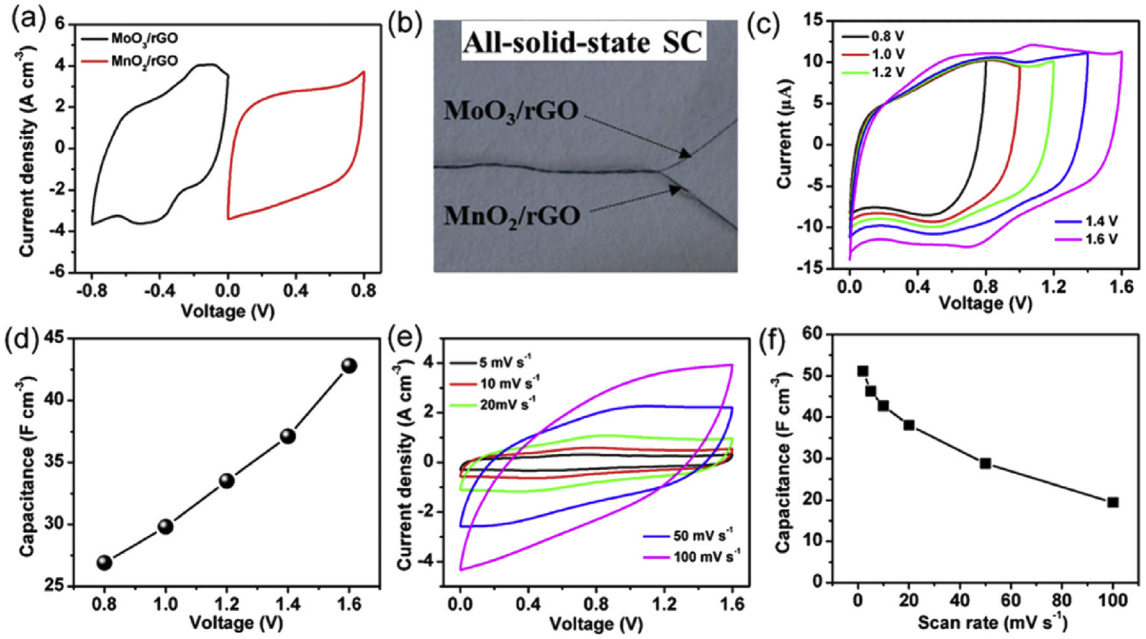

Fig. 6. (a) Comparative CV curves of MoO_3/rGO-60 fiber and MnO_2/rGO electrodes in a three-electrode cell in 1 M H_2SO_4. (b) An asymmetric fiber-shaped supercapacitor based on graphene/MnO_2 fiber as positive and graphene/MoO_3 as negative electrode. (c) CV curves of the ASC at different scan voltage windows. (d) Volumetric capacitance as the function of voltage windows. (e) CV curves at various scan rates. (f) The specific capacitance at different scan rates. (A colour version of this figure can be viewed online.)

increases to 4000 mA cm^{-3} a high capacitance of 26.3 F cm^{-3} could be maintained, indicating its good rate capability.

The power and energy density of the ASC were calculated from its galvanostatic discharge curves, and their relationship was depicted using Ragone plots (Fig. 7a). The ASC possesses a volumetric energy density of 18.2 mWh cm^{-3} at a power density of 76.4 mW cm^{-3}, which is about two times higher than the thin-film lithium battery and outperforms many other commercial devices. The volumetric energy density of our device is also higher than recently reported fiber-based SCs, including CNT/rGO fiber [29], MnO_2/carbon fibers [49,50], PEDOT/MWCNT fiber [51] and MoS_2-rGO/MWCNT fiber [52]. Besides its high energy density, our ASC exhibits outstanding power density (3269 mW cm^{-3}), which is comparable to the commercial SCs. In addition, our device exhibits good cycling performance with a capacitance retention of 96.8% after 3000 cycles of charge/discharge at a fixed current density of 1 A cm^{-3} (Fig. 7b). The flexibility and mechanical stability of the fiber-based SCs is very important in practical applications. The CV curves of our device in Fig. 7c have almost no obvious change under different bending angles, indicating its good robustness and mechanical stability.

4. Conclusions

In summary, we have successfully prepared MoO_3 nanorods/rGO and MnO_2 nanorods/rGO hybrid fibers by using a facile scalable wet-spinning method. Due to the synergetic effects between transition metal oxide nanorods and rGO, the capacitive performances of the hybrid fiber electrodes were improved. By using MnO_2 nanorods/rGO and MoO_3 nanorods/rGO hybrid fibers as the positive and negative electrodes, respectively, an all-solid-state ASC was constructed. The optimized ASC can be cycled reversibly at a high voltage of 1.6 V and deliver a superior volumetric energy density. Besides, the device exhibits remarkable cycling stability and excellent flexibility and mechanical stability. Owing to these outstanding performances, our device may provide promising applications in various flexible electronic devices.

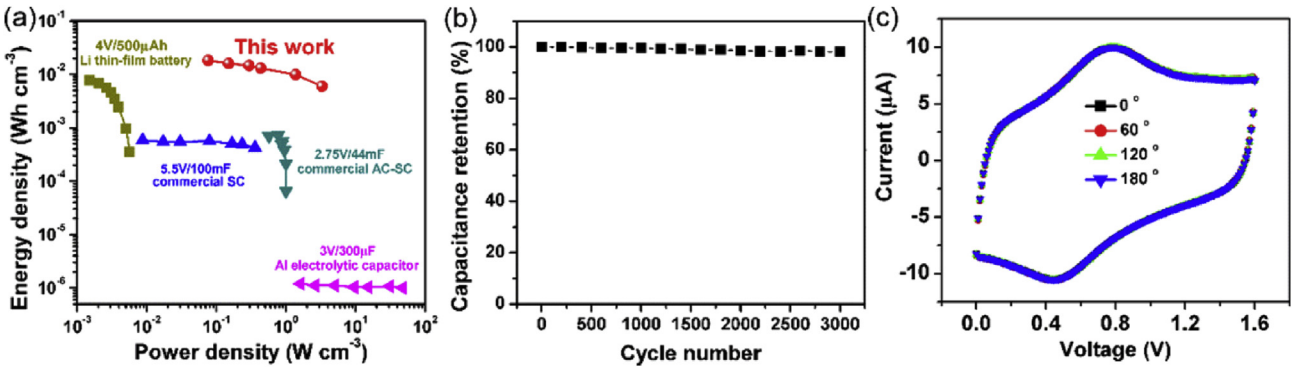

Fig. 7. (a) Ragone plots of our ASC and commercial energy-storage devices. (b) Cycle life of our ASC device. (c) CV curves at various bending angles. (A colour version of this figure can be viewed online.)

Acknowledgements

We acknowledge the financial supports from Natural Science Foundation of China (51273040, 51673038) and National Natural Science Foundation for Distinguished Young Scholar of China (50925312).

Appendix A. Supplementary data

Supplementary data related to this article can be found at http://dx.doi.org/10.1016/j.carbon.2016.11.051.

References

[1] X. Lu, M. Yu, G. Wang, Y. Tong, Y. Li, Flexible solid-state supercapacitors: design, fabrication and applications, Energy Environ. Sci. 7 (7) (2014) 2160–2181.
[2] B.C. Kim, J.-Y. Hong, G.G. Wallace, H.S. Park, Recent progress in flexible electrochemical capacitors: electrode materials, device configuration, and functions, Adv. Energy Mater. 5 (22) (2015) 1500959.
[3] L. Li, Z. Wu, S. Yuan, X. Zhang, Advances and challenges for flexible energy storage and conversion devices and systems, Energy Environ. Sci. (2014) 2101–2122.
[4] J. Fu, D.U. Lee, F.M. Hassan, L. Yang, Z. Bai, M.G. Park, et al., Flexible high-energy polymer-electrolyte-based rechargeable zinc–air batteries, Adv. Mater. 27 (37) (2015) 5617–5622.
[5] H. Lin, W. Weng, J. Ren, L. Qiu, Z. Zhang, P. Chen, et al., Twisted aligned carbon nanotube/silicon composite fiber anode for flexible wire-shaped lithium-ion battery, Adv. Mater. 26 (8) (2014) 1217–1222.
[6] G. Sun, X. Wang, P. Chen, Microfiber devices based on carbon materials, Mater. Today 18 (4) (2015) 215–226.
[7] X. Xiao, T. Li, Z. Peng, H. Jin, Q. Zhong, Q. Hu, et al., Freestanding functionalized carbon nanotube-based electrode for solid-state asymmetric supercapacitors, Nano Energy 6 (0) (2014) 1–9.
[8] P.J. Hall, M. Mirzaeian, S.I. Fletcher, F.B. Sillars, A.J.R. Rennie, G.O. Shitta-Bey, et al., Energy storage in electrochemical capacitors: designing functional materials to improve performance, Energy Environ. Sci. 3 (9) (2010) 1238–1251.
[9] J. Ren, W.Y. Bai, G.Z. Guan, Y. Zhang, H.S. Peng, Flexible and weaveable capacitor wire based on a carbon nanocomposite fiber, Adv. Mater. 25 (41) (2013) 5965–5970.
[10] H. Sun, X. You, J.E. Deng, X.L. Chen, Z.B. Yang, J. Ren, et al., Novel graphene/carbon nanotube composite fibers for efficient wire-shaped miniature energy devices, Adv. Mater. 26 (18) (2014) 2868–2873.
[11] D. Yu, K. Goh, H. Wang, L. Wei, W. Jiang, Q. Zhang, et al., Scalable synthesis of hierarchically structured carbon nanotube-graphene fibres for capacitive energy storage, Nat. Nano 9 (7) (2014) 555–562.
[12] S.-H. Lee, R.B. Ambade, S.B. Ambade, R.R. Salunkhe, V. Malgras, S.-H. Jin, et al., Flexible-wire shaped all solid-state supercapacitors based on facile electropolymerization of polythiophene with ultra-high energy density, J. Mater. Chem. A (2016) 7406–7415.
[13] J. Bae, M.K. Song, Y.J. Park, J.M. Kim, M. Liu, Z.L. Wang, Fiber supercapacitors made of nanowire-fiber hybrid structures for wearable/flexible energy storage, Angew. Chem. Int. Ed. 50 (7) (2011) 1683–1687.
[14] X. Zhang, Y. Lai, M. Ge, Y. Zheng, K.-Q. Zhang, Z. Lin, Fibrous and flexible supercapacitors comprising hierarchical nanostructures with carbon spheres and graphene oxide nanosheets, J. Mater. Chem. A 3 (24) (2015) 12761–12768.
[15] W. Ma, S. Chen, S. Yang, W. Chen, W. Weng, M. Zhu, Bottom-up fabrication of activated carbon fiber for all-solid-state supercapacitor with excellent electrochemical performance, ACS Appl. Mater. Inter. 8 (23) (2016) 14622–14627.
[16] G. Sun, X. Zhang, R. Lin, B. Chen, L. Zheng, X. Huang, et al., Weavable, high-performance, solid-state supercapacitors based on hybrid fibers made of sandwiched structure of MWCNT/rGO/MWCNT, Adv. Electron. Mater. 2 (7) (2016) 1600102.
[17] N. Zhang, W. Zhou, Q. Zhang, P. Luan, L. Cai, F. Yang, et al., Biaxially stretchable supercapacitors based on the buckled hybrid fiber electrode array, Nanoscale 7 (29) (2015) 12492–12497.
[18] Z. Xu, C. Gao, Graphene chiral liquid crystals and macroscopic assembled fibres, Nat. Commun. 2 (2011) 571.
[19] Z.L. Dong, C.C. Jiang, H.H. Cheng, Y. Zhao, G.Q. Shi, L. Jiang, et al., Facile fabrication of light, flexible and multifunctional graphene fibers, Adv. Mater. 24 (14) (2012) 1856–1861.
[20] S.H. Aboutalebi, R. Jalili, D. Esrafilzadeh, M. Salari, Z. Gholamvand, S. Aminorroaya Yamini, et al., High-performance multifunctional graphene yarns: toward wearable all-carbon energy storage textiles, ACS Nano 8 (3) (2014) 2456–2466.
[21] Y.N. Meng, Y. Zhao, C.G. Hu, H.H. Cheng, Y. Hu, Z.P. Zhang, et al., All-graphene core-sheath microfibers for all-solid-state, stretchable fibriform supercapacitors and wearable electronic textiles, Adv. Mater. 25 (16) (2013) 2326–2331.
[22] S. Chen, W. Ma, Y. Cheng, Z. Weng, B. Sun, L. Wang, et al., Scalable non-liquid-crystal spinning of locally aligned graphene fibers for high-performance wearable supercapacitors, Nano Energy 15 (2015) 642–653.
[23] L. Kou, T. Huang, B. Zheng, Y. Han, X. Zhao, K. Gopalsamy, et al., Coaxial wet-spun yarn supercapacitors for high-energy density and safe wearable electronics, Nat. Commun. 5 (2014) 3754.
[24] S. Chen, W. Ma, H. Xiang, Y. Cheng, S. Yang, W. Weng, et al., Conductive, tough, hydrophilic poly(vinyl alcohol)/graphene hybrid fibers for wearable supercapacitors, J. Power Sources 319 (2016) 271–280.
[25] W. Ma, S. Chen, S. Yang, M. Zhu, Hierarchically porous carbon black/graphene hybrid fibers for high performance flexible supercapacitors, RSC Adv. 6 (55) (2016) 50112–50118.
[26] J. Chang, M. Jin, F. Yao, T.H. Kim, V.T. Le, H. Yue, et al., Asymmetric supercapacitors based on graphene/MnO_2 nanospheres and graphene/MoO_3 nanosheets with high energy density, Adv. Funct. Mater. 23 (40) (2013) 5074–5083.
[27] M. Yu, Z. Wang, Y. Han, Y. Tong, X. Lu, S. Yang, Recent progress in the development of anodes for asymmetric supercapacitors, J. Mater. Chem. A (2016) 4634–4658.
[28] B. Zheng, T. Huang, L. Kou, X. Zhao, K. Gopalsamy, C. Gao, Graphene fiber-based asymmetric micro-supercapacitors, J. Mater. Chem. A 2 (25) (2014) 9736–9743.
[29] D. Yu, K. Goh, Q. Zhang, L. Wei, H. Wang, W. Jiang, et al., Controlled functionalization of carbonaceous fibers for asymmetric solid-state micro-supercapacitors with high volumetric energy density, Adv. Mater. 26 (39) (2014) 6790–6797.
[30] J. Liu, L. Zhang, H.B. Wu, J. Lin, Z. Shen, X.W. Lou, High-performance flexible asymmetric supercapacitors based on a new graphene foam/carbon nanotube hybrid film, Energy Environ. Sci. 11 (2014) 3709–3719.
[31] S. Peng, L. Li, H.B. Wu, S. Madhavi, X.W. Lou, Controlled growth of $NiMoO_4$ nanosheet and nanorod arrays on various conductive substrates as advanced electrodes for asymmetric supercapacitors, Adv. Energy. Mater. 5 (2) (2015) 1401172.
[32] X. Xiao, T. Ding, L. Yuan, Y. Shen, Q. Zhong, X. Zhang, et al., Wo_{3-x}/MoO_{3-x} core/shell nanowires on carbon fabric as an anode for all-solid-state asymmetric supercapacitors, Adv. Energy Mater. 2 (11) (2012) 1328–1332.
[33] W. Ma, S. Chen, S. Yang, W. Chen, Y. Cheng, Y. Guo, et al., Hierarchical MnO_2 nanowire/graphene hybrid fibers with excellent electrochemical performance for flexible solid-state supercapacitors, J. Power Sources 306 (2016) 481–488.
[34] Q. Chen, Y. Meng, C. Hu, Y. Zhao, H. Shao, N. Chen, et al., MnO_2-modified hierarchical graphene fiber electrochemical supercapacitor, J. Power Sources 247 (0) (2014) 32–39.
[35] G. Sun, J. Liu, X. Zhang, X. Wang, H. Li, Y. Yu, et al., Fabrication of ultralong hybrid microfibers from nanosheets of reduced graphene oxide and transition-metal dichalcogenides and their application as supercapacitors, Angew. Chem. 126 (46) (2014) 12784–12788.
[36] P. Yang, Y. Ding, Z. Lin, Z. Chen, Y. Li, P. Qiang, et al., Low-cost high-performance solid-state asymmetric supercapacitors based on MnO_2 nanowires and Fe_2O_3 nanotubes, Nano Lett. 14 (2) (2014) 731–736.
[37] W.S. Hummers, R.E. Offeman, Preparation of graphitic oxide, J. Am. Chem. Soc. 80 (6) (1958), 1339–1339.
[38] M.T. Greiner, M.G. Helander, W.-M. Tang, Z.-B. Wang, J. Qiu, Z.-H. Lu, Universal energy-level alignment of molecules on metal oxides, Nat. Mater. 11 (1) (2012) 76–81.
[39] A. Sumboja, C.Y. Foo, X. Wang, P.S. Lee, Large areal mass, flexible and free-standing reduced graphene oxide/manganese dioxide paper for asymmetric supercapacitor device, Adv. Mater. 25 (20) (2013) 2809–2815.
[40] Z. Xu, Y. Zhang, P.G. Li, C. Gao, Strong, conductive, lightweight, neat graphene aerogel fibers with aligned pores, ACS Nano 6 (8) (2012) 7103–7113.
[41] L. Noerochim, J.-Z. Wang, D. Wexler, Z. Chao, H.-K. Liu, Rapid synthesis of free-standing MoO_3/graphene films by the microwave hydrothermal method as cathode for bendable lithium batteries, J. Power Sources 228 (2013) 198–205.
[42] X. Yang, H. Ding, D. Zhang, X. Yan, C. Lu, J. Qin, et al., Hydrothermal synthesis of MoO_3 nanobelt-graphene composites, Cryst. Res. Technol. 46 (11) (2011) 1195–1201.
[43] X. Cao, B. Zheng, W. Shi, J. Yang, Z. Fan, Z. Luo, et al., Reduced graphene oxide-wrapped MoO_3 composites prepared by using metal–organic frameworks as precursor for all-solid-state flexible supercapacitors, Adv. Mater. 27 (32) (2015) 4695–4701.
[44] X. Wang, B. Liu, R. Liu, Q. Wang, X. Hou, D. Chen, et al., Fiber-based flexible all-solid-state asymmetric supercapacitors for integrated photodetecting system, Angew. Chem. Int. Ed. 53 (7) (2014) 1849–1853.
[45] G. Huang, C. Hou, Y. Shao, B. Zhu, B. Jia, H. Wang, et al., High-performance all-solid-state yarn supercapacitors based on porous graphene ribbons, Nano Energy 12 (2015) 26–32.
[46] C. Yang, J. Shen, C. Wang, H. Fei, H. Bao, G. Wang, All-solid-state asymmetric supercapacitor based on reduced graphene oxide/carbon nanotube and carbon fiber paper/polypyrrole electrodes, J. Mater. Chem. A 2 (5) (2014) 1458–1464.
[47] Z. Zhang, F. Xiao, S. Wang, Hierarchically structured MnO_2/graphene/carbon fiber and porous graphene hydrogel wrapped copper wire for fiber-based flexible all-solid-state asymmetric supercapacitors, J. Mater. Chem. A 3 (21) (2015) 11215–11223.
[48] X. Lu, M. Yu, T. Zhai, G. Wang, S. Xie, T. Liu, et al., High energy density asymmetric quasi-solid-state supercapacitor based on porous vanadium

nitride nanowire anode, Nano Lett. 13 (6) (2013) 2628–2633.
[49] X. Xiao, T. Li, P. Yang, Y. Gao, H. Jin, W. Ni, et al., Fiber-based all-solid-state flexible supercapacitors for self-powered systems, ACS Nano 6 (10) (2012) 9200–9206.
[50] N. Yu, H. Yin, W. Zhang, Y. Liu, Z. Tang, M.-Q. Zhu, High-performance fiber-shaped all-solid-state asymmetric supercapacitors based on ultrathin MnO_2 nanosheet/carbon fiber cathodes for wearable electronics, Adv. Energy Mater. 6 (2015) 1501458.
[51] J.A. Lee, M.K. Shin, S.H. Kim, H.U. Cho, G.M. Spinks, G.G. Wallace, et al., Ultrafast charge and discharge biscrolled yarn supercapacitors for textiles and microdevices, Nat. Commun. 4 (2013) 1970.
[52] G. Sun, X. Zhang, R. Lin, J. Yang, H. Zhang, P. Chen, Hybrid fibers made of molybdenum disulfide, reduced graphene oxide, and multi-walled carbon nanotubes for solid-state, flexible, asymmetric supercapacitors, Angew. Chem. 127 (15) (2015) 4734–4739.